HHS Public Access

Author manuscript

Artif Organs. Author manuscript; available in PMC 2021 May 01.

Published in final edited form as:

Artif Organs. 2020 May ; 44(5): E201–E213. doi:10.1111/aor.13609.

The Impact of Shear Stress on Device-Induced Platelet Hemostatic Dysfunction Relevant to Thrombosis and Bleeding in Mechanically Assisted Circulation

Zengsheng Chen[1,*], **Jiafeng Zhang**[1], **Tieluo Li**[1], **Douglas Tran**[1], **Bartley P. Griffith**[1], **Zhongjun Wu**[1,2]

[1]Department of Surgery, University of Maryland School of Medicine, Baltimore, MD, 21201, USA

[2]Fischell Department of Bioengineering, A. James Clark School of Engineering, University of Maryland, College Park, MD 20742, USA

Abstract

The aim of this study was to examine the impact of the non-physiological shear stress (NPSS) on platelet hemostatic function relevant to thrombosis and bleeding in mechanically assisted circulation. Fresh human blood was circulated for four hours in *in-vitro* circulatory flow loops with a CentriMag blood pump operated under a flow rate of 4.5 L/min against three pressure heads (70 mmHg, 150 mmHg and 350 mmHg) at 2100, 2800 and 4000 rpm, respectively. Hourly blood samples from the CentriMag pump-assisted circulation loops were collected and analyzed for glycoprotein (GP) IIb/IIIa activation and receptor shedding of GPVI and GPIbα on the platelet surface with flow cytometry. Adhesion of platelets to fibrinogen, collagen and von Willebrand factor (VWF) of the collected blood samples was quantified with fluorescent microscopy. In parallel, mechanical shear stress fields within the CentriMag pump operated under the three conditions were assessed by computational fluid dynamics (CFD) analysis. The experimental results showed that levels of platelet GPIIb/IIIa activation and platelet receptor shedding (GPVI and GPIbα) in the blood increased with increasing the circulation time. The levels of platelet activation and loss of platelet receptors GPVI and GPIbα were consistently higher with higher pressure heads at each increasing hour in the CentriMag pump-assisted circulation. The platelet adhesion on fibrinogen increased with increasing the circulation time for all three CentriMag operating conditions and was correlated well with the level of platelet activation. In contrast, the platelet adhesion on collagen and VWF decreased with increasing the circulation time under all the three conditions and was correlated well with the loss of the receptors GPVI and GPIbα on the platelet surface, respectively. The CFD results showed that levels of shear stresses inside the CentriMag pump under all three operating conditions exceeded the maximum level of shear stress in the normal physiological circulation and were strongly dependent of the pump operating condition. The level of platelet activation and loss of key platelet adhesion receptors (GPVI and

Correspondence: Zhongjun J. Wu, Ph.D., Department of Surgery, University of Maryland School of Medicine, 10 South Pine Street, MSTF 434A, Baltimore, MD, 21201, USA, Tel: 410-706-7715, Fax: 410-706-0311, zwu@som.umaryland.edu.

[*]**Current Address:** Beijing Advanced Innovation Center for Biomedical Engineering, Beihang University, Beijing, 100083, China, School of Biological Science and Medical Engineering, Beihang University, Beijing, 100083, China

Declaration of Interest statement

All other authors declare that they have no conflict of interest in the subject matter or materials discussed in this study.

GPIbα) were correlated with the level of NPSS generated by the CentriMag pump, respectively. In summary, the level of NPSS associated with pump operating condition is a critical determinant of platelet dysfunction in mechanically assisted circulation.

Keywords

platelet receptor shedding; non-physiological shear stress; mechanical circulatory support; bleeding; thrombosis

Introduction

Mechanical circulatory support (MCS) is a device-based therapy to sustain the blood circulation for patients whose heart does not work properly on its own. The most clinical used MCS devices include ventricular assist devices (VAD), pump-oxygenators used for extracorporeal membrane oxygenation (ECMO) and heart-lung machines for cardiopulmonary bypass. The clinical application of MCS provides the vital perfusion to and maintains functioning of all organs. Despite the significant progress in MCS clinical use, the MCS therapy is not free of undesirable consequences. The significant complications with MCS, such as thrombosis and bleeding, were associated with worsening morbidity and mortality [1–5]. Almost all contemporary MCS devices employ a rotary blood pump to pump the blood in the circulation. The high-speed rotation of the impeller in rotary blood pumps generates high non-physiological shear stress (NPSS) [6]. Song et al. reported that shear stresses along the blade-tip surface of a centrifugal VAD can reach 250 Pa [7]. Fraser et al. found that shear stresses in the impeller bladed regions of an axial VAD can rise beyond 1000 Pa [8]. In our previous study, we found that the level of NPSS in the HVAD centrifugal blood pump increased with increasing rotational speed of the impeller [9].

Blood through rotary blood pumps inevitably encounters NPSS. It has been well-known that NPSS can stretch red blood cells (RBCs) and eventually cause breakage of RBCs' membrane leading to hemolysis [10]. It has been also well-recognized that high shear stress could induce platelet activation, leading to pathological thrombosis [11, 12]. Shankaran et al. reported that when platelets were sheared at 9600 s^{-1} for 5 min, 46% of them can be activated [12]. We also found that NPSS (125 Pa) could induce remarkable platelet activation even with very short exposure time (0.5 sec) [13]. The excessive activation of platelets can promote further recruitments of additional platelets to adhesion and aggregation at the site of injured vascular [14]. In addition, NPSS can also induce damage to other blood elements and coagulation factors, such as fragmentation of high molecular weight multimers of von Willebrand factor (VWF) [15, 16], and damage to leukocytes [17].

Platelets play pivotal roles in physiologic and pathologic processes of hemostasis. The initiation and formation of the platelet plug at injury sites is the important first step for hemostatic process. Although platelet activation is one critical step for hemostasis, overactivated platelets in blood stream may cause disorders of hemostasis leading to the increased risk of thrombosis. Besides the shear-induced platelet activation, high shear stress can induce platelet receptor shedding. We and other groups recently demonstrated that NPSS could induce loss of key platelet receptors, especially the GPIbα and GPVI [18–22]. The

interactions of platelet receptor GPIbα with VWF and platelet receptor GPVI with collagen are crucial steps to form initial platelet plugs for the hemostatic process at the sites of vascular injury. The loss of GPIbα and GPVI could result in defective platelet-substrate adhesion, impairing physiological hemostasis, and increase the potential of bleeding.

At present, there are several clinical configurations of MCS for different clinical scenarios and treatment purposes. The required pressure heads for a rotary blood pump are different. For example, the CentriMag centrifugal pump has been used for temporary ventricular support and ECMO support. The device-generated pressure head (ΔP) could be around 75 mmHg for extracorporeal right ventricular support device or fully implantable LVAD. However, the required pressure head could be as high as 350 mmHg for veno-arterial (VA) ECMO support. The shear stress levels are different for different clinical operating conditions, which could cause different levels of blood damage. In this study, the effects of device-generated NPSS on platelets and relevant hemostasis function were investigated. The CentriMag blood pump was operated to provide MCS under three clinically relevant operating conditions: a blood flow rate of 4.5 L/min with pump pressure heads of 75 mmHg, 150 mmHg and 350 mmHg. These three operating conditions represent three clinical MCS applications: permanent LVAD support, temporary extracorporeal LVAD support and VA ECMO support, respectively. Three in-vitro mechanically assisted circulation loops with the CentriMag blood pump (Abbott, Pleasanton, CA) were built to mimic the three clinical support scenarios. Computational fluid dynamics (CFD) simulation was performed to analyze mechanical shear stresses generated by the CentriMag pump in these loops. Computationally derived NPSS were associated with the observed platelet activation and receptor shedding of the in-vitro experiments.

Materials and methods

Reagents

V450 labeled Anti-Human CD41a (CD41a-V450) (platelet identification), BV510-labeled anti-Human CD42b (CD42b-BV510) (GPIbα quantification) and isotype control BV510 conjugated IgG1K (IgG1K-BV510), fluorescein isothiocyanate (FITC)-labeled anti-human PAC-1 (PAC-1 FITC) (platelet activation) and isotype control FITC conjugated IgMK (IgMK-FITC) were purchased from BD Biosciences (San Jose, CA, USA). efluor 660-labeled anti-human GPVI (GPVI-efluor 660) and isotype control efluor 660 conjugated IgG1K (IgG1K-efluor 660) were purchased from eBioscience (San Diego, CA, USA). HEPES buffer was purchase from Corning (NY, USA). Human plasma fibrinogen and human plasma VWF were purchased from EMD Millipore (Billerica, MA, USA). Human collagen (Type I) was purchased from Chrono-log (Havertown, PA, USA).

Blood Collection

This study was approved by the Institutional Review Board of the University of Maryland, Baltimore and in compliance with the Declaration of Helsinki. Human blood was collected from 8 healthy donors (4 men and 4 women with age range between 22 to 30 years) who had not taken any antiplatelet or anticoagulant medication two weeks before blood donation. All the donors were informed the aim of the study and gave their written informed consent.

From each donor, one unit (450 ml) of blood was drawn from the antecubital vein into a sterile collection bag containing 50 ml sodium citrate (ratio 9:1).

In Vitro Circulation Loop

Figure 1 shows a small volume circulatory loop with a small soft-shell reservoir. The loop was adapted from the work by Olia et al. [23] and consists of a CentriMag blood pump, a reservoir, a resistance clamp, and 3/8" tubing (Medtronic, Minneapolis, MN). All tubing and blood bags were medical grade with acceptable biocompatibility. Blood was drawn by the CentriMag blood pump and was propelled through the resistance clamp into the small-volume blood reservoir. The pump speed and the flow resistance of the circulatory loop were adjusted to achieve the required condition of flow rate and pump pressure head (ΔP). The inlet and outlet pressure of the CentriMag blood pump was measured by calibrated piezoelectric pressure transducers (Model 1502B01EZ5V20GPSI, PCB Piezotronics, Inc., Depew, NY, USA). The volumetric flow rate was measured with a transonic flow meter with a clamp-on probe (T401/ME9PXL, Transonic System, Ithaca, NY).

Experimental procedure

The three loops with the CentriMag pump that represent three clinical MCS scenarios were operated under the following conditions: 1) Loop 1 representing the permanent LVAD support, flow rate Q = 4.5 L/min, ΔP = 75 mmHg and impeller speed Ω = 2100 rpm; 2) Loop 2 representing the temporary extracorporeal LVAD support, Q = 4.5 L/min, ΔP = 150 mmHg and Ω = 2800 rpm; 3) Loop 3 representing the VA ECMO support, Q = 4.5 L/min, ΔP = 350 mmHg and Ω = 4000 rpm. Two of the three conditions were tested with one blood donation at the same time. The hematocrit of the collected blood was adjusted to 30% ± 2% by hemodilution with 0.5% bovine serum albumin (BSA) [24]. The conditioned blood was then divided equally by volume and added into two identical circulatory loops. Before loading blood sample, we utilized phosphate buffer saline (PBS) to rinse the whole circulated loop. After PBS rinsing, the blood sample was gently loaded into the mock loop. Blood in the loops were circulated continuously for 4 hours. Baseline blood samples were collected from each loop before the circulation was initiated. Then blood samples were collected hourly for flow cytometric analysis and other measurements. The experimental run for each loop was repeated at least six times.

Sample preparation for flow cytometry analysis

For analysis of platelet activation, 5 μl whole blood samples were incubated with a mixture containing 25 μl HEPES buffer, 20 μl PAC-1 FITC or IgMK-FITC and 5 μl CD41a-V450 for 30 min at room temperature (RT) in the dark. For analysis of GPVI shedding, 5 μl whole blood samples were incubated with a mixture containing 25 μl HEPES buffer, 5 μl GPVI-efluor 660 or IgG1K-eFluor 660 and 5 μl CD41a-V450 for 30 min at RT in the dark. For analysis of GPIbα shedding, 5 μl whole blood samples were incubated with a mixture containing 25 μl HEPES buffer, 5 μl CD42b-BV510 or IgG1K-BV510 and 5 μl CD41a-V450 for 30min at RT in the dark. All the prepared samples were fixed with 1% paraformaldehyde (PFA) (1 ml) for 30 min at 4°C in the dark. Then, the flow cytometry data for the samples were acquired by a flow cytometer (FACSVerse, BD Bioscience, San Jose,

CA) and analyzed with the FCS Express software (De Novo Software, Los Angeles, CA, USA).

Platelet adhesion on immobilized fibrinogen, collagen and VWF

Platelet adhesion assays were performed using micro glass tubes (0.2 mm X 2 mm X 25 mm, VitroCom, Mountain Lakes, NJ). These tubes were individually coated overnight at 4°C with fibrinogen (1 mg/ml), collagen (1 mg/ml) or VWF (100 μg/ml), and blocked with 5% BSA in PBS at RT for 2 hours followed by PBS rinse. The collected blood samples were incubated with 10 μM mepacrine (quinacrine dihydrochloride, Sigma, St. Louis, MO) for 20 min in the dark at RT to fluorescently label platelets. The previous studies had shown that when a final concentration for mepacrine <20 μM was used, it would not affect platelet function [25, 26]. Mepacrine-treated blood was perfused through the protein-coated glass tubes at a shear rate of 500 s^{-1} for 5 min in the dark using a syringe pump (Harvard PHD2000, Harvard Apparatus, MA, USA). Then, nonattached cells were removed by gently rinsing 3 times with PBS. The remaining adherent platelets were fixed with 3.7% PFA and imaged using a fluorescence microscope (IX71, Olympus) equipped with an Olympus DP80 digital camera. Finally, ten images with 2 mm interval along the center axis of each glass tube were taken and used to calculate the average area covered by adhered platelets on each tube using custom-written software in MATLAB (Natick, MA, USA).

Computational fluid dynamics simulation

The geometry of the CentriMag blood pump was retrieved from the computer aided drawing (CAD) files. Commercial software Ansys (Ansys, Inc, Canonsburg, PA, USA) was used to construct the model of the blood flow domain and to conduct the CFD simulation. Motion of the impellers was incorporated using the multiple reference frame approach. For the comparison purpose to the in-vitro experimental results, the CentriMag impeller rotating speeds and flow rate were selected to be the same as the in-vitro experiments. The K-ω shear stress transport turbulence model was chosen to solve the flow field. Blood was treated as an incompressible Newtonian fluid with a viscosity of 3.5 mPa•s and a density of 1050 kg/m^3. The boundary conditions were set as: **a)** a uniform flow (4.5 L/min) at the inlet entrance, and **b)** the outflow condition at the outlet exit. Both the inlet and outlet were extended to ensure the fully developed flow and avoid the boundary impact. The mesh independent analysis was carried out to ensure that the CFD simulation results were independent of further mesh refinement. The mesh elements used in this study were 7.34 million. During the CFD simulation, the calculation was considered convergent when **1)** the residuals of the continuity, momentum and turbulence equations were below 10^{-3}; **2)** the difference between the flow rates at the inlet and outlet was less than 5%; and 3) pressure at the inlet approached a constant value. The scalar shear stress (SSS) used in this study was calculated with the following formula [6, 8]:

$$\sigma = \left[\frac{1}{6} \sum_{i \neq j} (\tau_{ii} - \tau_{jj})^2 + \sum_{i \neq j} \tau_{ij}^2 \right]^{1/2}$$

where τ_{ij} is the shear stress tensor, which can be derived from the CFD solved velocity fields. More details of CFD setup and mesh independence analysis can be found in our previous publications [6, 9] [27].

Statistical analysis

The experimental data were presented as mean ± SE (standard error of the mean). The comparisons of the data at the baseline and post-circulation time points among the three operating conditions were carried out using the two-way repeated measures ANOVA with a Fisher's Least Significant Difference (LSD) post hoc test (Prism, GraphPad Software, San Diego, CA). The blood sampling time and the CentriMag pump operating condition were the main factors. Regression analysis was performed to determine and compare the rates of change in measured parameters with respect to the blood circulation time among the three operating conditions. A *P*-value of less than 0.05 was considered to be statistically significant.

Results

Platelet activation and receptor shedding

As shown in Figure 2A, platelet GPIIb/IIIa activation (indicated by PAC-1 FITC binding) increased with increasing the circulation time in the three circulatory loops. For Loop 1 (75 mmHg), platelet activation increased from 0.97% in the baseline blood sample to 1.02%, 1.25%, 1.76% and 1.95% in the four post-circulation blood samples. For Loop 2 (150 mmHg), platelet activation increased from 1.09% in the baseline blood sample to 3.20%, 4.85%, 7.16% and 10.86% in the four post-circulation blood samples. For Loop 3 (350 mmHg), platelet activation increased from 1.06% in the baseline blood sample to 4.55%, 6.75%, 9.32% and 15.77% in the four post-circulation blood samples. Compared to baseline sample, platelet activation became significant in Loop 1 after three hours of the CentriMag blood pump-assisted circulation. For both Loop 2 and Loop 3, platelet activation was statistically significant after one hour of the pump-assisted circulation compared to the baseline samples. Among the three loops, the level of platelet activation increased with the rising ΔP for the same circulating time. Both Loop 2 and Loop 3 caused significantly higher platelet activation than Loop 1 for the same circulating time. Platelet activation in Loop 3 was slightly higher than Loop 2 for the same circulation time. The regression analysis indicated that the increasing rates of platelet activation in Loop 2 and Loop 3 were significantly higher than that in Loop1. The differences in the increasing rate of platelet activation between Loop 2 and Loop 3 was not statistically significant.

Figure 2B and 2C show the expression levels of platelet GPVI and GPIbα in the baseline and four post-circulation blood samples from the three circulatory loops. The data were presented as the normalized mean fluorescence intensity (MFI) of fluorophore-conjugated antibodies bound to the GPVI and GPIbα receptors on the platelet surface. Since the MFI is proportional to fluorophores-conjugated to the antibody bound to available receptors on the platelet surface, the MFI can represent the relative quantity of the receptors of GPVI and GPIbα on the platelet surface. As shown in Figure 2B, the normalized MFI of the GPVI surface expression decreased with increasing the circulation time for all three loops. In Loop

1, the GPVI expression decreased by 2.1%, 4.5%, 5.8% and 7% in the four post-circulation blood samples compared to the baseline sample, respectively. For Loop 2, the reduction in the GPVI expression was 3.5%, 7.5%, 11.9% and 17.2% in the four post-circulation blood samples, respectively. For Loop 3, the reduction in the GPVI expression was 14.7%, 25.2%, 30.1% and 38.6% in the four post-circulation blood samples compared to the baseline sample, respectively. For all the three loops, the reduction in the GPVI expression in the four post-circulation blood samples was significant compared to the baseline blood sample. At all four sampling time points after the pump-assisted circulation, the reduction in the GPVI expression was higher in a loop with a higher ΔP, the lowest in Loop 1 and the highest in Loop 3. The regression analysis indicated that the reduction rates of the GPVI expression statistically different among the three loops.

Similar to the observation of the reduction in the GPVI expression, the GPIbα surface expression also decreased in each loop with increasing the circulation time. The reduction in the GPIbα expression increased with increasing ΔP among the three loops at the same sampling time (Fig. 2C). For Loop 1, the reduction in the GPIbα expression was 2.7%, 5.5%, 8.7% and 9.5% in the four post-circulation blood samples compared to the baseline blood sample. For Loop 2, the reduction in the GPIbα expression was 4.8%, 8.3%, 13.0% and 16.1% in the four post-circulation blood samples. For Loop 3, the reduction in the GPIbα expression was 10.5%, 14%, 18.9% and 24.8% in the four post-circulation blood samples. The reduction in the GPIbα expression became significant in the blood samples from Loop 1 at two hours after initiation of the circulation compared to the baseline blood sample, while the reduction in the GPIbα expression for Loop 2 and Loop 3 were significant at one hour after initiation of the circulation. Among the three loops, the reduction in the GPIbα expression was the highest in Loop 3 and the lowest in Loop 1. The regression analysis indicated that the reduction rates of the GPIbα expression in Loop 2 and Loop 3 were statistically higher than that in Loop1. The difference in the reduction rate between Loop 2 and Loop 3 was not statistically different.

Alteration of platelet adhesion to fibrinogen, collagen and VWF

Figure 3A shows representative images of platelets adhered on fibrinogen for the baseline and two hourly collected blood samples from the three loops. Figure 3B shows the normalized values of the platelet coverage on the fibrinogen-coated surface to the baseline blood sample for the collected blood samples from the three loops. It was clearly that significantly more platelets adhered to fibrinogen with increasing the circulation time for all the three loops. The platelet surface coverage on fibrinogen for the four post-circulation blood samples increased 1.6, 1.8, 2.1 and 2.4 folds for Loop 1 after 1, 2, 3, 4 hours of the circulation, respectively. The differences in the platelet coverage on fibrinogen between different time points were not statistically different. The platelet surface coverage on fibrinogen for the four post-circulation blood samples increased 2.3, 3.1, 4.0 and 5.0 folds for Loop 2 and 5.0, 5.9, 8.4, 10.0 folds for Loop 3 at 1, 2, 3, and 4 hours, respectively. Significant increase of platelet adhesion on fibrinogen was observed at two hours after the circulation compared to baseline sample. In contrast, the platelet adhesion on fibrinogen for Loop 3 increased significantly after one hour. For all the three loops, the platelet adhesion on fibrinogen was higher in a loop with a higher ΔP. The increase in the platelet adhesion on

fibrinogen was the highest in Loop 3 and the lowest in Loop 1 at any sampling time point. The regression analysis indicated that the rates of the increase in the platelet adhesion on fibrinogen were statistically different for the three loops.

Figure 4A shows representative images of platelets adhered on collagen for the baseline and two hourly collected blood samples from the three loops. It can be seen from the images that the number of platelets adhered on collagen decreased with the circulation time in the three loops. The degree of the decrease in the number of platelets adhered on collagen was more severe in the loop with the higher ΔP. Figure 4B shows the normalized values of the platelet coverage on the collagen-coated surface to the baseline blood sample for the collected blood samples from the three loops. The surface coverage of platelets adhered on collagen decreased by 11.2%, 25.8%, 35.8% and 42.7% from to the baseline after 1, 2, 3, and 4 hours of the pump-assisted circulation in Loop 1. The reduction of the surface area coverage by platelets on collagen became significant after two hours of the circulation in Loop 1. The surface coverage of platelets adhered on collagen decreased by 40.2%, 52.4%, 67.37% and 74.1% in Loop 2 and by 58.8%, 77.1%, 83.7% and 85.8% in Loop 3 after 1, 2, 3 and 4 hours of the pump-assisted circulation, respectively. The reduction in platelet adhesion on collagen became statistically significant after 1 hour of the circulation in both Loop 2 and Loop 3. The regression analysis indicated that the rates of the reduction in platelet adhesion on collagen were statistically different during the first hours of the pump-assisted circulation among the three loops. Thereafter, the rates of the reduction in platelet adhesion on collagen appeared to be not significantly different.

Similar to the observation of the altered platelet adhesion on collagen, platelet adhesion on VWF also decreased with the circulation time. Figure 5A shows representative images platelets adhered on VWF for the baseline and two hourly collected blood samples from the three loops. The degree of the decrease in the number of platelets adhered on VWF was also more severe in the loop with the higher ΔP. Figure 5B shows the normalized values of the platelet coverage on the VWF-coated surface to the baseline blood sample for the collected blood samples from the three loops. The surface coverage of platelets adhered on collagen decreased by 14.5%, 33.4%, 40.5% and 51% from the baseline after 1, 2, 3, and 4 hours of the pump-assisted circulation in Loop 1. The reduction of the surface area coverage by platelets on collagen became significant after two hours of the circulation in Loop 1. The reduction was 22.1%, 39.8%, 50.4% and 58.7% in Loop 2 and 34.7%, 55%, 66.1% and 73.3% in Loop 3 after 1, 2, 3 and 4 hours of the pump-assisted circulation, respectively. In all the three loops, the blood exhibited significantly reduced platelet adhesion on VWF compared to their baseline samples. The regression analysis indicated that the rates of the reduction in platelet adhesion on VWF were statistically different during the first hours of the pump-assisted circulation. Thereafter, the rates of the reduction in platelet adhesion on VWF appeared to be very similar.

Shear stresses generated by the CentriMag pump in three loops

Figure 6 shows computationally simulated wall shear stress (WSS) contours on the impeller surface of the CentriMag pump (Figure 6A) and scalar shear stress (SSS) contours on two cut-through planes of the pump chamber under the operating conditions in the three loops

(Figure 6B). As expected, areas on the impeller surface with high WSS (red) increased with increasing rotational speed to generate the required high ΔP. The area weighted average WSS values on the impeller were 36.4, 53.9 and 98.2 Pa for Loop 1, Loop 2 and Loop 3, respectively. The percentage of the areas with WSS higher than 125 Pa were 3.3%, 6.7% and 20.8% for Loop 1, 2 and 3, respectively. Similar to the trend of the WSS distribution on the impeller surface, regions with bulk high SSS (green to red) were larger with increasing rotational speed, i.e., high ΔP. The volume weighted average SSS values were 5.7, 7.28, and 11.16 Pa for Loop1, Loop 2 and Loop 3, respectively.

Association of platelet dysfunction with shear stress in pump-assisted circulation

Correlation analysis was performed to link pump-generated shear stresses through CFD simulation and experimentally measured platelet dysfunction parameters from the in-vitro experiments. Shear stress indices, including area weighted average WSS on the impeller, volume weighted average SSS inside the pump and averaged linear shear stress accumulation (LSA) along pathlines of particles, were derived from CFD-simulated flow fields for the CentriMag pump operating conditions in the three loops. LSA has been used as a semi-quantitative value to estimate platelet activation [28]. The structural alterations (activation and receptor shedding) and dysfunction (altered adhesion on fibrinogen, collagen and VWF) of platelets at 4 hours after the CentriMag pump-assisted circulation were used as the platelet dysfunctional parameters. Figure 7 shows trend lines of measured parameters for platelet activation, loss of GPVI and GPIbα receptors on the platelet surface and changes of platelet adhesion on fibrinogen, collagen and VWF versus the averaged SSS for the CentriMag pump operating conditions in the three loops. Table 1 lists the correlation coefficients between the three shear stress indices and the six measured platelet dysfunction parameters changes. It was found that the averaged SSS was the best among the three indicators.

Discussion

During the clinical mechanical circulatory support, the NPSS could be created by blood pump inevitably, which can bring damage on the important hemostatic cell, the platelet. The device-induced platelet damage in patients implanted with MCS had been reported by a previous study. Lukito et al. [29] examined the loss of platelet receptors occurring in patients with MCS, and reported that the elevated plasma GPVI levels and notably decreased GPIbα and GPVI receptors on platelet surface were found in continuous flow-VADs and ECMO patients compared to healthy donors. In this study, we want to investigate the impact of the level of NPSS generated by a rotary blood pump for MCS in device-induced platelet dysfunction. A pump-assisted extracorporeal circuit with a CentriMag blood pump was constructed with the pump operated to replicate three relevant clinical scenarios: fully implantable LVAD support (Loop 1), temporary extracorporeal LVAD support (Loop 2) and VA ECMO support (Loop 3), respectively. In the fully implantable LVAD support setting, a rotary pump is only required to generate a pressure head to overcome the pressure difference between the left ventricle and the aorta, which is typically around 75 mmHg [30, 31]. In contrast, long tubing will be used for temporary extracorporeal LVAD support and a blood oxygenator will be added for VA ECMO support. Because of the resistance created by the

long connecting tubing and the oxygenator, a rotary blood pump must be operated at higher rotational speeds to generate a pressure head to overcome the additional pressure loss across tubing and oxygenator. Thus, the ΔP required for a rotary blood pump for temporary extracorporeal HF support is higher than the fully implantable LVAD support. A pressure head of 150 mmHg was considered to be representative in the extracorporeal LVAD support setting. For a typical VA ECMO support, a pressure head of 350 mmHg is representative based on our clinical experience. Our CFD simulation results confirmed that NPSS levels increased with the increased pressure head, corresponding to the increased pump speed. The pump speed in Loop 3 was the highest, the percentage of blood cells exposed to NPSS was the largest in Loop 3 among the three loops. According to the CFD data, one may conclude that the device-induced platelet damage could be the most severe in Loop 3, suggesting that patient on VA ECMO support may be very vulnerable to device-induced platelet dysfunction.

Our experimental data clearly showed that the levels of platelet activation and receptor shedding caused by the pump operation were the highest for the blood samples collected from Loop 3, followed by Loop 2, and the least from Loop 1. Since the activated GPIIb/IIIa has high affinity with fibrinogen, more activated platelets could adhere on fibrinogen. This is consistent with that platelet adhesion on fibrinogen was the highest in the blood samples collected from Loop 3, followed by Loop 2, and the least from Loop 1. More platelet activation and more platelet adhesion on fibrinogen could lead to higher risk of thrombosis. The risk of thrombotic events for patients on ECMO support could be higher than those on fully implantable LVAD support. As reported by previous studies, the rate of thrombotic events in patients with permanent LVAD support (2.2% to 8%) [32, 33] was lower than that in patients on ECMO support (31% to 44%) [34, 35].

The bindings of platelet receptor GPVI with exposed collagen and platelet receptor GPIbα with immobilized VWF are the key steps for hemostasis in the event of vascular injury. The loss of GPVI and GPIbα on the platelet surface could reduce the platelet adhesion capacity. Our data showed that the blood samples from Loop 3 exhibited the most severe receptor shedding (loss) of GPVI and GPIbα and also the most severe reduction in platelet adhesion capacities on collagen and VWF. The blood sample from Loop 1 had the least receptor shedding of GPVI and GPIbα and the least reduction in platelet adhesion capacities on collagen and VWF. The loss of platelet receptor GPVI and GPIbα and the reduction of platelet adhesion on collagen and VWF could comprise hemostasis, increasing the risk of bleeding [36]. Our data implied that the risk of bleeding events for patients on ECMO support could be higher than patients on LVAD support. It has been reported that 70% of patients on ECMO support experienced bleeding events [34] while bleeding events occurred in only 30% patients on LVAD support (30%) [37]. These clinical reports are consistent with the data from our study.

Our experimental data showed that the pump-induced platelet damage was the most severe in Loop 3, similar to a setting of VA ECMO support, requiring a very high pump pressure. The severe platelet damage can be explained by the extreme NPSS generated by the high-speed rotation of the pump impeller under this condition. Pumps in the current ECMO systems often are required to generate a very high pressure to overcome the significant

circuit flow resistance by long tubing and current resistive oxygenators. Our study showed that lower pump pressure head is preferred to reduce shear-induced platelet damage. Therefore, an optimal ECMO circuit could be implemented by using short tubing and a low resistance oxygenator for lower flow resistance in the circuit. By doing so, a blood pump can operate at a lower speed to provide the same circulatory support, but generate lower NPSS, resulting in less platelet damage.

The CentriMag blood pump has been used as a temporary VAD or part of ECMO. Bleeding and thrombotic complications remain a leading cause of morbidity and mortality for patients on ECMO support [38–41]. It is commonly believed that device alters hemostatic function by producing a hypercoagulable state of platelets and coagulation system leading to the increased thrombotic risk, while anticoagulation is responsible for the increased bleeding risk. However, this cannot explain why patients with ECMO or LVAD support suffer concurrent thrombotic and bleeding risks. As indicated by our study, in the patient implanted with a MCS device, NPSS generated by the device can cause two opposite effects on platelets: one is to induce the platelet activation, which can increase the platelet adhesion with fibrinogen leading to elevated risk of thrombosis; and the other is to cause platelet receptor shedding (GPVI and GPIbα), which can reduce the platelet adhesion capacities on hemostasis related proteins (collagen and VWF) leading to elevated propensity of bleeding events. Although only a small portion of blood cells are exposed to the extreme NPSS in the CentriMag pump, the blood passes continuously through the pump. The effect of NPSS on platelets can be accumulated gradually. Therefore, the number of activated platelets can increase and correspondingly the adhesion capacity of platelet on fibrinogen can be heightened. In parallel, the shedding of platelet receptors (GPVI and GPIbα) and the reduction of platelet adhesion with collagen and VWF increase with the circulation time and continued exposure to NPSS.

In the present study, it was observed that CFD-derived shear stress indices (average SSS, average WSS, and LSA) were well correlated with the levels of platelet activation, platelet receptor shedding, and altered platelet adhesion capacities in the three loops. However, the average SSS was the best indicator for the pump-induced platelet damage and dysfunction. Although average WSS was higher than the volume average SSS, only a very small portion of platelets may pass though the regions adjacent to the impeller surface. Therefore, the WSS has limited impact on shear-induced platelet dysfunction compared to the overall flow domain. The volume weighted average SSS represents the overall shear stress level of the flow domain that majority platelets are exposed to. Although LSA represents the combined effects of SSS and exposure time, only limited number of platelet particles could be tracked, which means limited regions of the pumps are covered by LSA. Therefore, the correlation between LSA and platelet dysfunction levels are not as good as expected. This study suggested that the volume weighted average SSS can be a good indicator to estimate pump-induced blood damaged. This may help to guide the blood pump design optimization.

Conclusion

The present study demonstrated that the level of blood pump-generated NPSS had a direct impact on platelet activation and receptor shedding in mechanically assisted circulation. The

level of platelet activation and receptor shedding was almost linear to the volume weighted average SSS from CFD simulation. The pump-generated NPSS-induced platelet damage (activation and receptor shedding) affected the platelet adhesion on fibrinogen, collagen and VWF. The adhesion of NPSS-damaged platelets on fibrinogen increased with the NPSS level and the circulation time while the adhesion of NPSS-damaged platelets on collagen and VWF decreased with the circulation time. The observation of the concurrent platelet activation and receptor shedding caused by the CentriMag pump in the circulatory flow loops may explain the existence of the more severe current thrombotic and bleeding events in patients on certain MCS, such as ECMO, that requires a higher pump pressure. The data from the study suggest that lowering the rotational speed of a rotary blood pump in ECMO circuit may potentially lower platelet injury caused by the pump rotation.

Acknowledgments

Research reported in this publication was supported by the National Heart, Lung, and Blood Institute of the National Institutes of Health (Award Numbers: R01HL118372, R01HL124170, and R01HL141817).

References

1. Meyer AL, Kuehn C, Weidemann J, Malehsa D, Bara C, Fischer S, et al. Thrombus formation in a HeartMate II left ventricular assist device. J Thorac Cardiovasc Surg. 2008;135(1):203–204. [PubMed: 18179943]
2. Eckman PM, John R. Bleeding and thrombosis in patients with continuous-flow ventricular assist devices. Circulation. 2012;125(24):3038–3047. [PubMed: 22711669]
3. Koliopoulou A, McKellar SH, Rondina M, Selzman CH. Bleeding and thrombosis in chronic ventricular assist device therapy: focus on platelets. Curr Opin Cardiol. 2016;31(3):299–307. [PubMed: 27054505]
4. Crow S, John R, Boyle A, Shumway S, Liao K, Colvin-Adams M, et al. Gastrointestinal bleeding rates in recipients of nonpulsatile and pulsatile left ventricular assist devices. J Thorac Cardiovasc Surg. 2009;137(1):208–215. [PubMed: 19154927]
5. Blitz A Pump thrombosis-A riddle wrapped in a mystery inside an enigma. Ann Cardiothorac Surg. 2014;3(5):450–471. [PubMed: 25452905]
6. Chen Z, Jena SK, Giridharan GA, Koenig SC, Slaughter MS, Griffith BP, Wu ZJ. Flow features and device-induced blood trauma in CF-VADs under a pulsatile blood flow condition: A CFD comparative study. Int J Numer Method Biomed Eng. 2018;34(2). doi: 10.1002/cnm.2924.
7. Song X, Throckmorton AL, Wood HG, Antaki JF, Olsen DB. Quantitative evaluation of blood damage in a centrifugal VAD by computational fluid dynamics. Journal of fluids engineering. 2004;126(3):410–418.
8. Fraser KH, Zhang T, Taskin ME, Griffith BP, Wu ZJ. A quantitative comparison of mechanical blood damage parameters in rotary ventricular assist devices: shear stress, exposure time and hemolysis index. J Biomech Eng. 2012;134(8):081002. [PubMed: 22938355]
9. Chen Z, Jena SK, Giridharan GA, Sobieski MA, Koenig SC, Slaughter MS, Griffith BP, Wu ZJ. Shear stress and blood trauma under constant and pulse-modulated speed CF-VAD operations: CFD analysis of the HVAD. Med Biol Eng Comput. 2019;57(4):807–818. [PubMed: 30406881]
10. Baskurt OK, Meiselman HJ. Red blood cell mechanical stability test. Clin Hemorheol Microcirc. 2013;55(1):55–62. [PubMed: 23445627]
11. Casa LD, Deaton DH, Ku DN. Role of high shear rate in thrombosis. J Vasc Surg. 2015;61(4):1068–1080. [PubMed: 25704412]
12. Shankaran H, Alexandridis P, Neelamegham S. Aspects of hydrodynamic shear regulating shear-induced platelet activation and self-association of von Willebrand factor in suspension. Blood. 2003 4 1;101(7):2637–45. [PubMed: 12456504]

13. Chen Z, Mondal NK, Ding J, Koenig SC, Slaughter MS, Griffith BP, et al. Activation and shedding of platelet glycoprotein IIb/IIIa under non-physiological shear stress. Mol Cell Biochem. 2015;9(1–2):93–101.
14. Koupenova M, Kehrel BE, Corkrey HA, Freedman JE. Thrombosis and platelets: an update. European heart journal. 2017;38(11):785–791. [PubMed: 28039338]
15. Proudfoot AG, Davidson SJ, Strueber M. von Willebrand factor disruption and continuous-flow circulatory devices. J Heart Lung Transplant. 2017;36(11):1155–1163. [PubMed: 28756118]
16. Tsai HM. von Willebrand factor, shear stress, and ADAMTS13 in hemostasis and thrombosis. ASAIO journal. 2012;58(2):163–169. [PubMed: 22370688]
17. Dewitz TS, Hung TC, Martin RR, McIntire LV. Mechanical trauma in leukocytes. J Lab Clin Med. 1977;90(4):728–736. [PubMed: 903701]
18. Al-Tamimi M, Tan CW, Qiao J, Pennings GJ, Javadzadegan A, Yong AS, et al. Pathologic shear triggers shedding of vascular receptors: a novel mechanism for down-regulation of platelet glycoprotein VI in stenosed coronary vessels. Blood. 2012;119(18):4311–4320. [PubMed: 22431567]
19. Chen Z, Koenig SC, Slaughter MS, Griffith BP, Wu ZJ. Quantitative Characterization of Shear-Induced Platelet Receptor Shedding: Glycoprotein Ibalpha, Glycoprotein VI, and Glycoprotein IIb/IIIa. ASAIO journal. 2018;64(6):773–778. [PubMed: 29117043]
20. Chen Z, Mondal NK, Ding J, Gao J, Griffith BP, Wu ZJ. Shear-induced platelet receptor shedding by non-physiological high shear stress with short exposure time: glycoprotein Ibalpha and glycoprotein VI. Thrombosis research. 2015;135(4):692–698. [PubMed: 25677981]
21. Chen Z, Mondal NK, Ding J, Koenig SC, Slaughter MS, Wu ZJ. Paradoxical Effect of Non-physiological Shear Stress on Platelets and von Willebrand Factor. Artificial organs. 2016;40(7):659–668. [PubMed: 26582038]
22. Cheng H, Yan R, Li S, Yuan Y, Liu J, Ruan C, et al. Shear-induced interaction of platelets with von Willebrand factor results in glycoprotein Ibalpha shedding. Am J Physiol Heart Circ Physiol. 2009;297(6):H2128–35. [PubMed: 19820200]
23. Olia SE, Herbertson LH, Malinauskas RA, Kameneva MV. A Reusable, Compliant, Small Volume Blood Reservoir for In Vitro Hemolysis Testing. Artificial organs. 2017;41(2):175–178. [PubMed: 27087363]
24. ASTM International. The Standard Practice for Assessment of Hemolysis in Continuous Blood Flow Pumps - ASTM F1841–97 (2017). Available from: www.astm.org/Standards/F1841.htm
25. Savage B, Saldívar E, Ruggeri ZM. Initiation of platelet adhesion by arrest onto fibrinogen or translocation on von Willebrand factor. Cell. 1996 1 26;84(2):289–97. [PubMed: 8565074]
26. Jamiolkowski MA et al., Real time visualization and characterization of platelet deposition under flow onto clinically relevant opaque surfaces. J Biomed Mater Res A. 2015;103(4):1303–11. [PubMed: 24753320]
27. Zhang J, Zhang P, Fraser KH, Griffith BP, Wu ZJ. Comparison and experimental validation of fluid dynamic numerical models for a clinical ventricular assist device. Artificial organs. 2013;37(4):380–389. [PubMed: 23441681]
28. Xenos M, Girdhar G, Alemu Y, Jesty J, Slepian M, Einav S, et al. Device Thrombogenicity Emulator (DTE)--design optimization methodology for cardiovascular devices: a study in two bileaflet MHV designs. Journal of biomechanics. 2010;43(12):2400–2409. [PubMed: 20483411]
29. Lukito P, Wong A, Jing J, Arthur JF, Marasco SF, Murphy DA, et al. Mechanical circulatory support is associated with loss of platelet receptors glycoprotein Ibα and glycoprotein VI. J Thromb Haemost. 2016;14(11):2253–2260. [PubMed: 27601054]
30. Haft J, Armstrong W, Dyke DB, Aaronson KD, Koelling TM, Farrar DJ, Pagani FD et al. Hemodynamic and exercise performance with pulsatile and continuous-flow left ventricular assist devices. Circulation. 2007;116(11 Suppl):I8–15. [PubMed: 17846330]
31. Teuteberg JJ, Slaughter MS, Rogers JG, McGee EC, Pagani FD, Gordon R, et al. The HVAD Left Ventricular Assist Device: Risk Factors for Neurological Events and Risk Mitigation Strategies. JACC Heart failure. 2015;3(10):818–828. [PubMed: 26450000]
32. Starling RC, Blackstone EH, Smedira NG. Increase in left ventricular assist device thrombosis. N Engl J Med. 2014;370(15):1465–1466.

33. Najjar SS, Slaughter MS, Pagani FD, Starling RC, McGee EC, Eckman P, et al. An analysis of pump thrombus events in patients in the HeartWare ADVANCE bridge to transplant and continued access protocol trial. J Heart Lung Transplant. 2014;33(1):23–34. [PubMed: 24418731]
34. Dalton HJ, Reeder R, Garcia-Filion P, Holubkov R, Berg RA, Zuppa A, et al. Factors Associated with Bleeding and Thrombosis in Children Receiving Extracorporeal Membrane Oxygenation. Am J Respir Crit Care Med. 2017;196(6):762–771. [PubMed: 28328243]
35. Dalton HJ, Garcia-Filion P, Holubkov R, Moler FW, Shanley T, Heidemann S, et al. Association of bleeding and thrombosis with outcome in extracorporeal life support. Pediatr Crit Care Med. 2015;16(2):167–174 [PubMed: 25647124]
36. Hu J, Mondal NK, Sorensen EN, Cai L, Fang HB, Griffith BP, et al. Platelet glycoprotein Ibalpha ectodomain shedding and non-surgical bleeding in heart failure patients supported by continuous-flow left ventricular assist devices. J Heart Lung Transplant. 2014;33(1):71–9. [PubMed: 24055626]
37. Stulak JM, Lee D, Haft JW, Romano MA, Cowger JA, Park SJ, et al. Gastrointestinal bleeding and subsequent risk of thromboembolic events during support with a left ventricular assist device. J Heart Lung Transplant. 2014;33(1):60–64. [PubMed: 24021944]
38. Oliver WC. Anticoagulation and coagulation management for ECMO. Semin Cardiothorac Vasc Anesth. 2009;13(3):154–175. [PubMed: 19767408]
39. Hastings SM, Ku DN, Wagoner S, Maher KO, Deshpande S. Sources of Circuit Thrombosis in Pediatric Extracorporeal Membrane Oxygenation. ASAIO journal. 2017;63(1):86–92. [PubMed: 27660905]
40. Brodie D, Bacchetta M. Extracorporeal membrane oxygenation for ARDS in adults. N Engl J Med. 2011;365(20):1905–1914. [PubMed: 22087681]
41. Haines NM, Rycus PT, Zwischenberger JB, Bartlett RH, Undar A. Extracorporeal Life Support Registry Report 2008: neonatal and pediatric cardiac cases. ASAIO journal. 2009;55(1):111–116. [PubMed: 19092657]

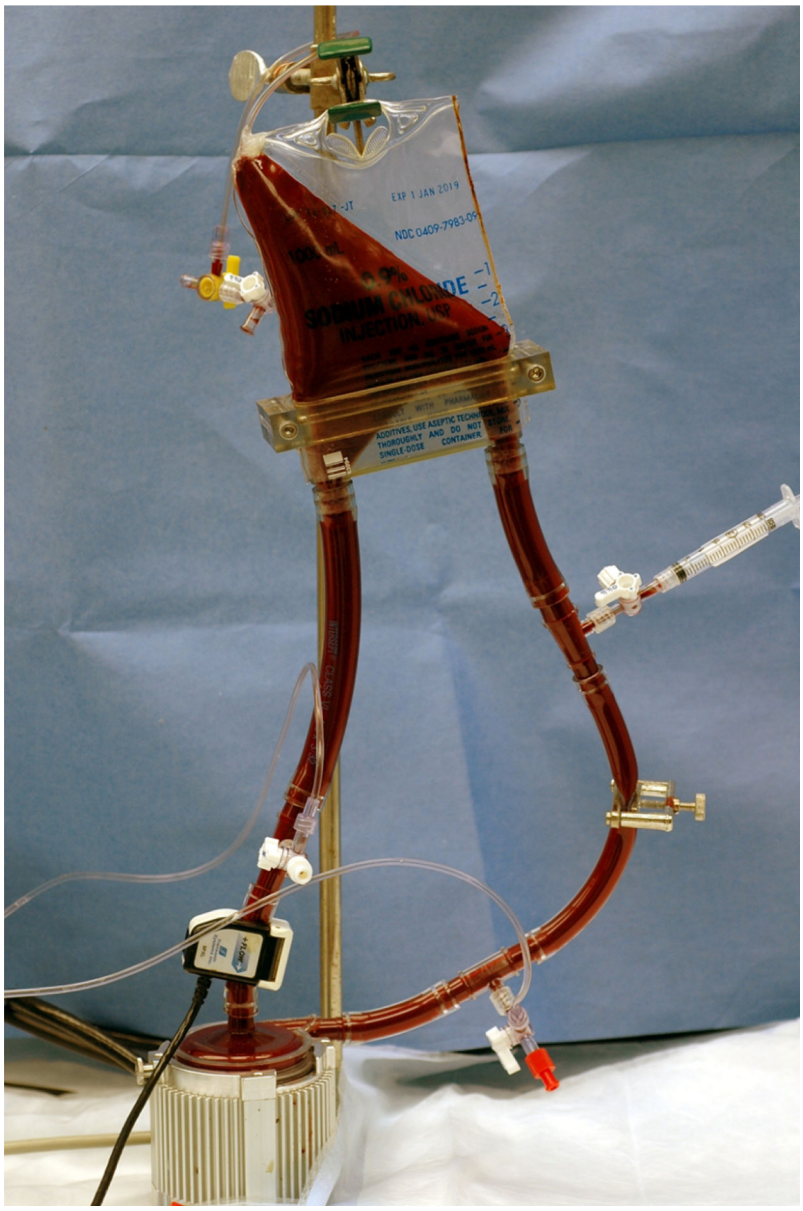

Figure 1.

Photograph of the small-volume *in vitro* circulation loop. This loop consists of a CentriMag blood pump, a soft-shell blood reservoir, medical tubing, resistance adjust clamps, ultrasonic flow probe, fluid-filled inlet and outlet pressure transducers.

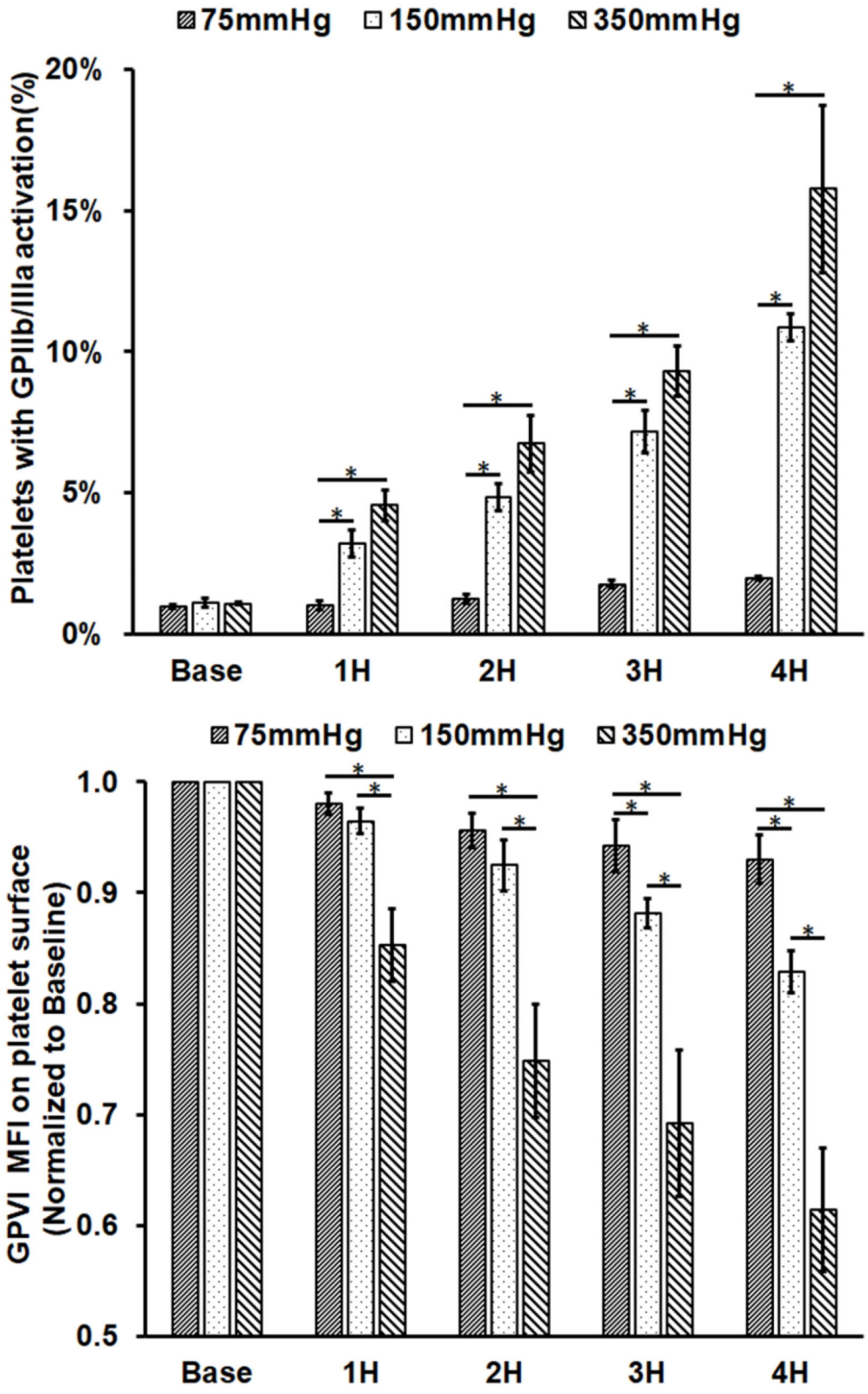

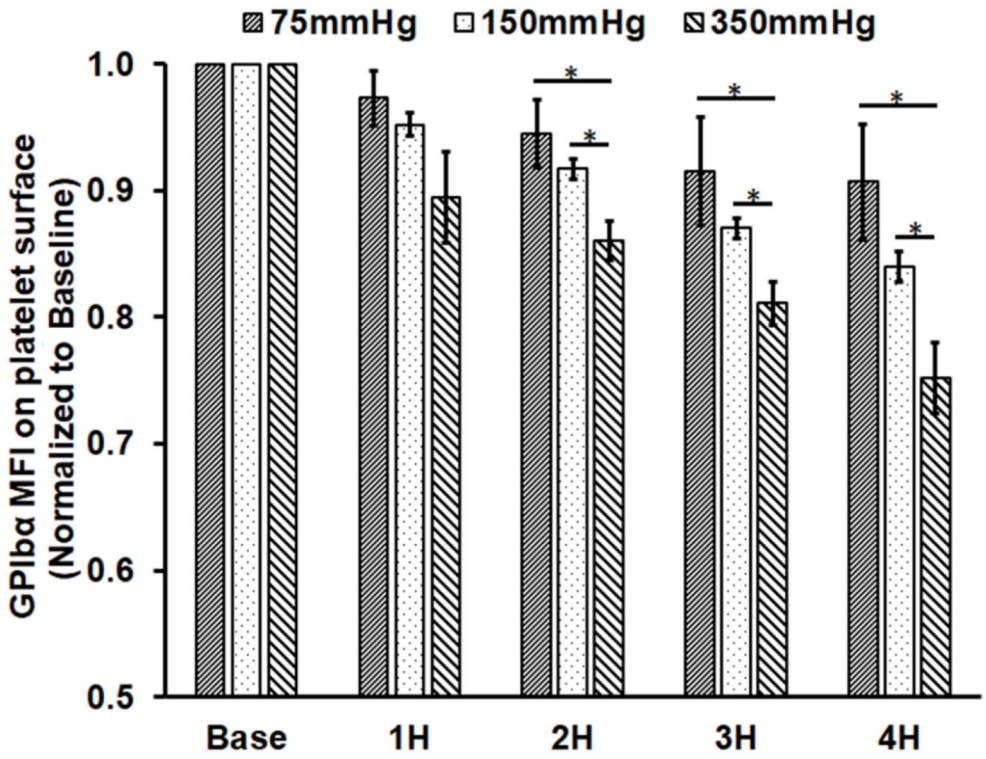

Figure 2.

Measured platelet activation and receptor shedding in the baseline and four hourly collected blood samples from the three circulation loops (ΔP=75 mmHg, 150 mmHg and 350 mmHg). **A)** The percentage of activated platelets (GPIIb/IIIa activation); **B)** the level of GPVI expression on the platelet surface in the platelet population; and **C)** the level of GPIbα expression on the platelet surface. The MFI for GPVI and GPIbα were normalized to the baseline blood sample (**P*<0.05).

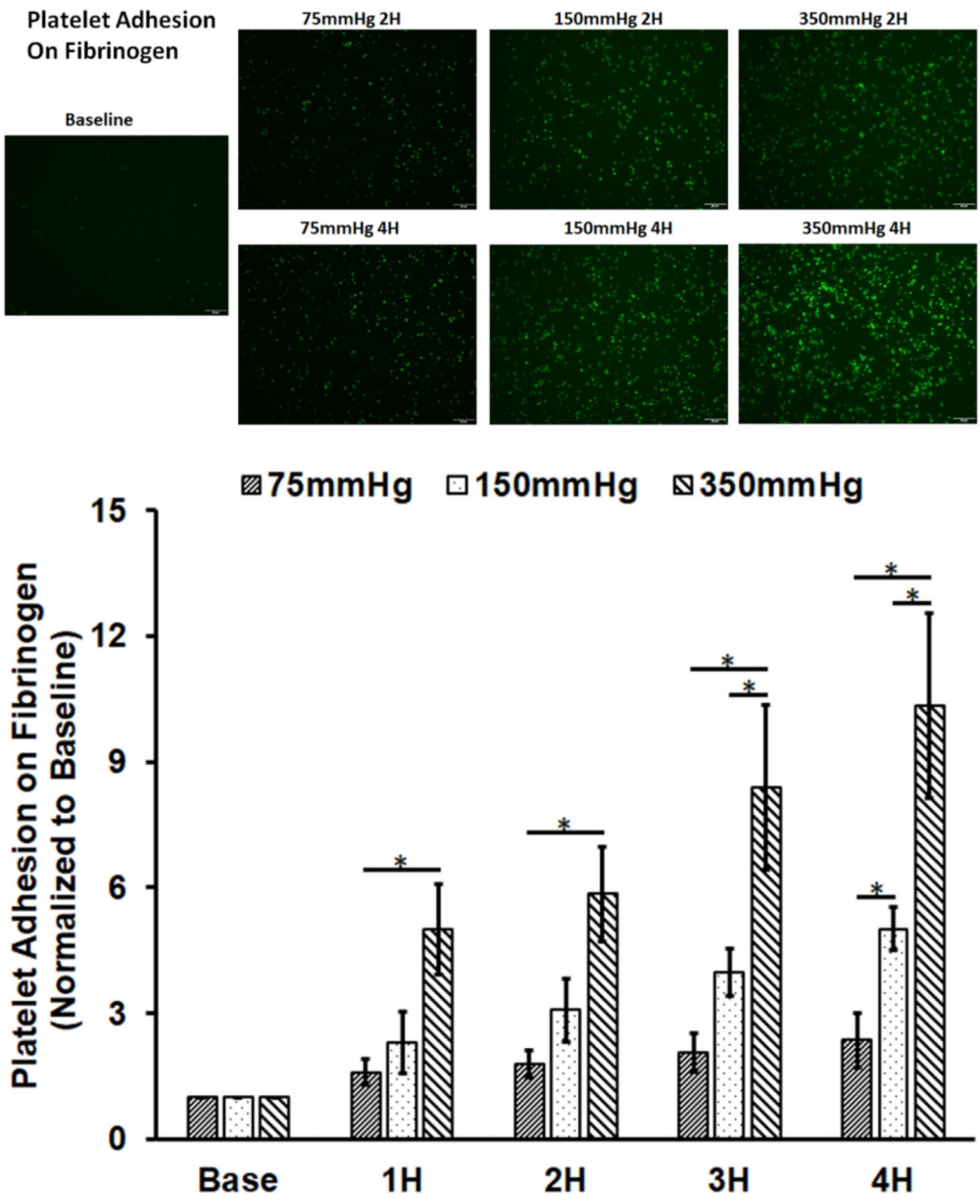

Figure 3.

Altered platelet adhesion on fibrinogen of the blood from the three loops (ΔP=75 mmHg, 150 mmHg and 350 mmHg). **A)** Representative images of platelet adhesion on fibrinogen from the baseline and two hourly blood samples (the 2nd and 4th hours) (magnification, X400); **B)** the quantitative comparison of the area coverage of adherent platelets on fibrinogen from the baseline and four hourly samples (**P*<0.05).

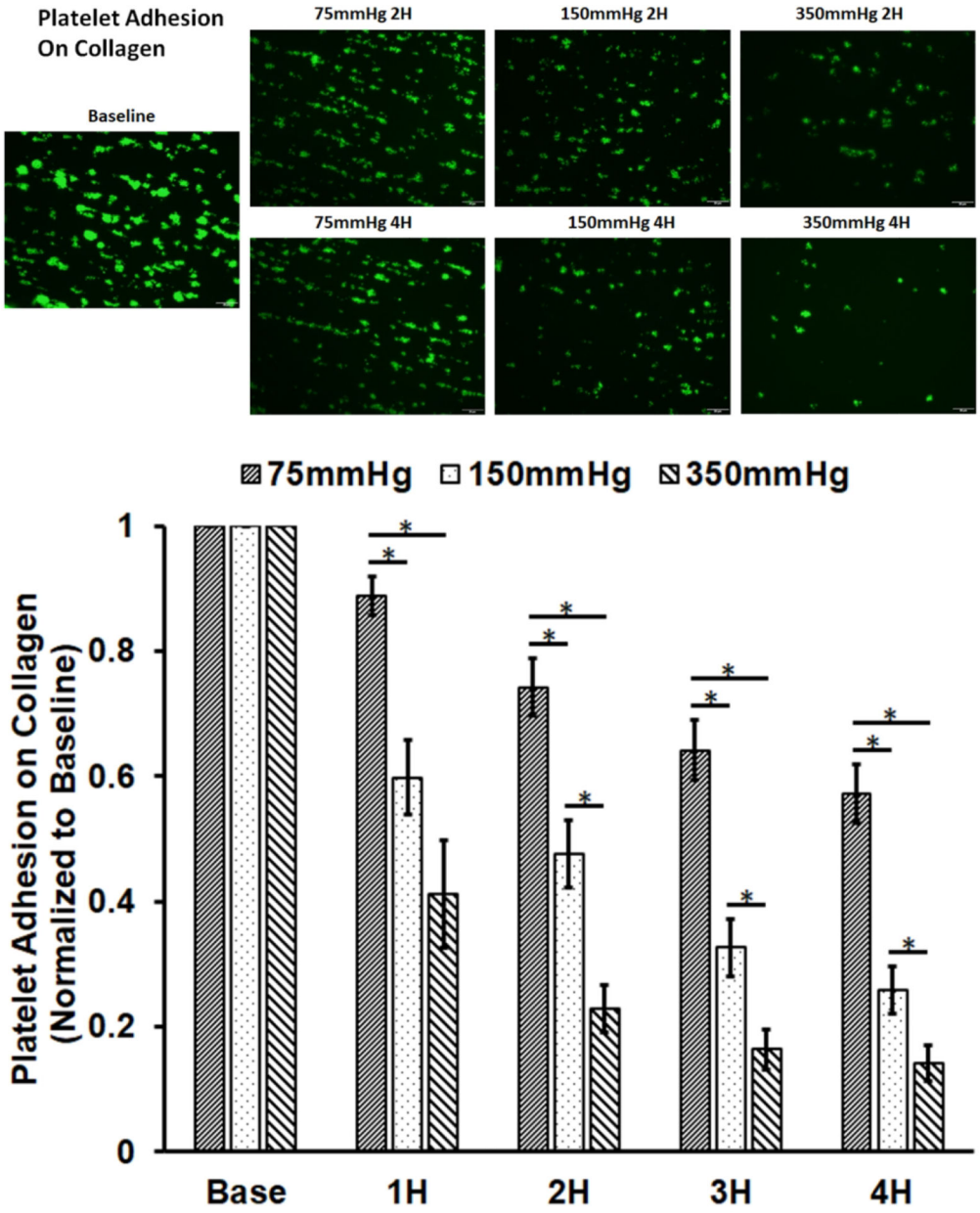

Figure 4.

Altered platelet adhesion on collagen of the blood from the three loops (ΔP=75 mmHg, 150 mmHg and 350 mmHg). **A)** Representative images of platelet adhesion on collagen from the baseline and two hourly blood samples (the 2nd and 4th hours) (magnification, X400); **B)** The quantitative comparison of the area coverage of adherent platelets on collagen from the baseline and four hourly samples (**P*<0.05).

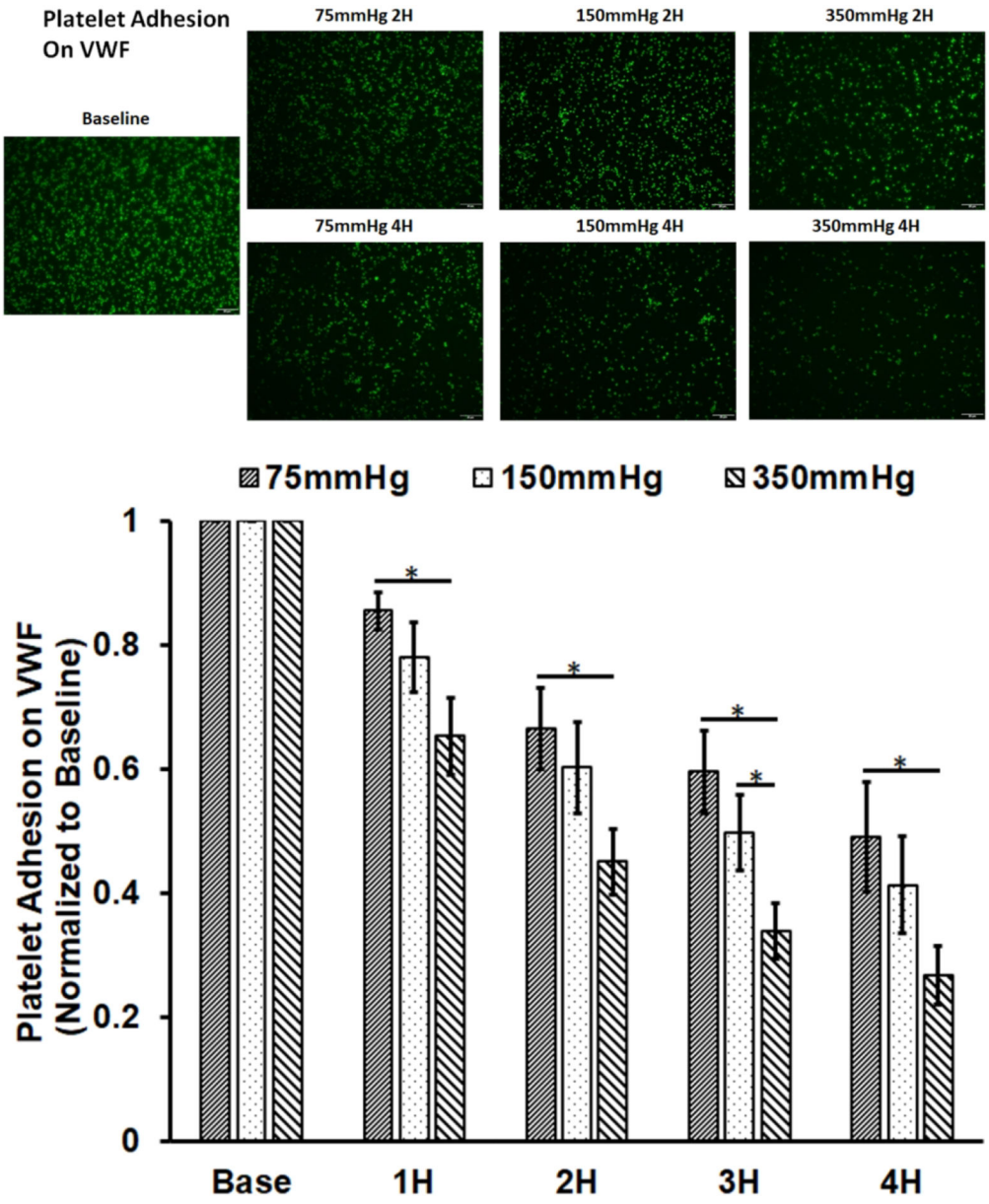

Figure 5.

Altered platelet adhesion on VWF of the blood from the three loops (ΔP=75 mmHg, 150 mmHg and 350 mmHg). **A)** Representative images of platelet adhesion on VWF from the baseline and two hourly blood samples (the 2nd and 4th hours) (magnification, X400); **B)** The quantitative comparison of the area coverage of adherent platelets on VWF from the baseline and four hourly samples (**P*<0.05).

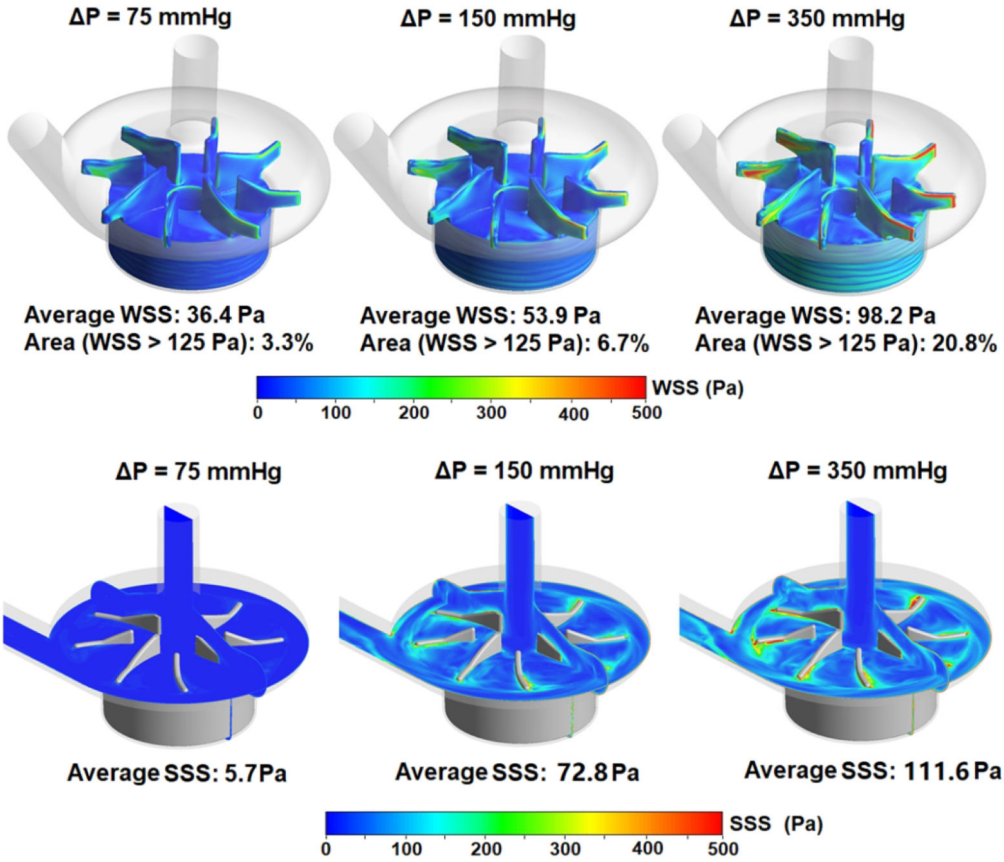

Figure 6.

A) Wall shear stress (WSS) contours on the impeller of the CentriMag blood pump under three operating conditions (4.5 L/min, 75 mmHg at 2100 rpm, 150 mmHg at 2800 rpm, 350 mmHg at 4000 rpm); and **B)** Scalar shear stress (SSS) distributions on two cut-through planes in the CentriMag pump chamber under the three operating conditions.

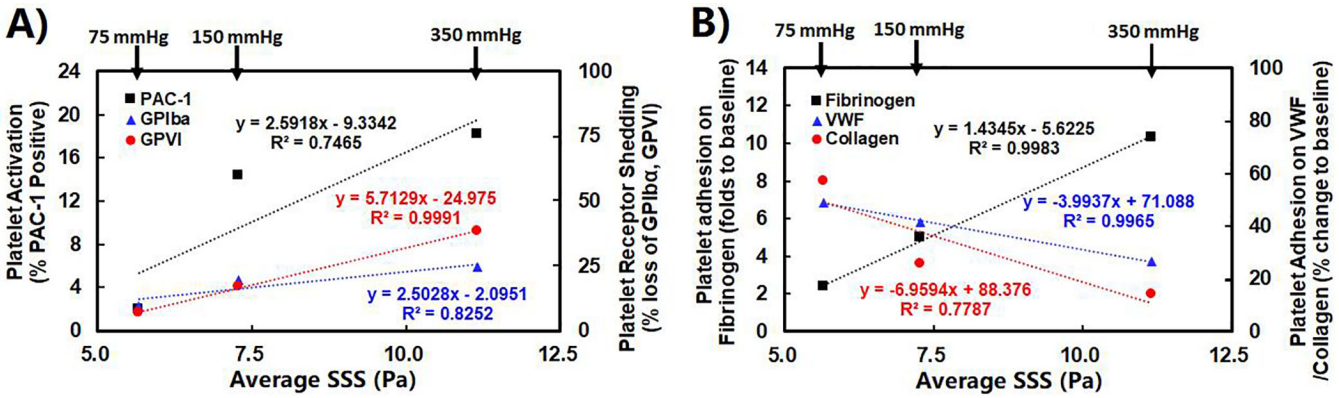

Figure 7.

A) The correlative relationships between the levels of platelet activation and receptor shedding and the average SSS in the CentriMag pump after 4-hour pump-assisted circulation; and **B)** the correlative relationships between the platelet adhesion on fibrinogen, VWF and collagen and the average SSS in the CentriMag Pump after 4-hour pump-assisted circulation.

Table 1.

Correlation coefficient (R^2) of shear stress indices and platelet dysfunction measures.

Platelet dysfunction parameter \ Shear stress index	Averaged WSS	Averaged SSS	Averaged LSA
GPIIb/IIIa activation	0.7308	0.7465	0.5509
The loss of GPIbα	0.8114	0.8252	0.6451
The loss of GPVI	0.9977	0.9991	0.9451
The adhesion of platelet on fibrinogen	0.9965	0.9983	0.9397
The adhesion of platelet on VWF	0.9941	0.9965	0.9311
The adhesion of platelet on collagen	0.7673	0.7787	0.5884